



OPEN

Impact of C- and N-terminal protection on the stability, metal chelation and antimicrobial properties of calcitermin

Maria D'Accolti¹, Denise Bellotti^{1,2}✉, Emilia Dzień², Carlotta Leonetti¹, Silvia Leveraro¹, Valentina Albanese³, Erika Marzola¹, Remo Guerrini¹, Elisabetta Caselli¹, Magdalena Rowińska-Żyrek² & Maurizio Remelli¹

The main limitation to the use of antimicrobial peptides (AMPs) as regular drugs, against antibiotic and antifungal resistance, mainly relates to their rapid degradation by proteolytic enzymes. The introduction of suitable structural changes in the peptide chain can make the peptide less susceptible to the action of proteases, thus overcoming this problem. To improve the plasma stability of calcitermin, a metal-chelating AMP present in the human respiratory tract and investigated in the present study, C- and/or N-terminal modifications have been introduced in the native sequence. Evaluation of peptide stability has been performed to determine the half-life times in human plasma of both native calcitermin and its derivatives. However, the protection of the peptide termini can also affect its metal coordination behaviour. Thus, the characterization of Zn²⁺ and Cu²⁺ complexes has been performed by means of several techniques, including potentiometry, high-resolution mass spectrometry, UV–Vis, circular dichroism and EPR. On the basis of the obtained results, it was possible to compare the biological activity of the studied systems, taking into account both the metal-binding ability and the peptide stability to search for a link among them. A significant result of this study is that the N-terminal protection increases the calcitermin half-life over seven times and the formation of metal complexes confers resistance towards degradation almost doubling its half-life.

Antimicrobial resistance (AMR) is one of the most important health challenges of the twenty-first century. Among several novel approaches aimed at overcoming the global drug-resistance crisis, the use of antimicrobial peptides (AMPs) represents a promising strategy for the design of new drugs¹. They exhibit a broad spectrum of activity, being effective against a wide variety of pathogens, like Gram-positive² and Gram-negative bacteria³, fungi⁴, viruses⁵ and even cancer cells⁵ and are present in all living organisms (invertebrates, vertebrates, plants, prokaryotes)⁶. However, these extraordinary candidate molecules present some drawbacks, the major one being the fact that they are metabolically unstable. The AMPs activity level is subject to modulation or degradation by both human and pathogenic proteolytic enzymes. In fact, many endo- and exo-peptidases act to transform high molecular weight peptides into shorter oligopeptides, making them inactive. This problem translates into short half-lives (usually less than 30 min) and scarce bioavailability⁷. Therefore, in order to improve the therapeutic potential of these molecules, a rational design of new AMP analogues is required with the aim of optimizing their chemical properties and the engineering of delivery systems⁸.

Calcitermin is a 15-mer peptide (VAIALKAAHYHTHKE, WT) corresponding to the C-terminal domain of calgranulin C, a pro-inflammatory protein of the S100 family. It contains an effective metal-binding domain with three alternated histidine residues in position 9, 11 and 13, and the free terminal amino and carboxyl groups⁹. The complex-formation equilibria of this natural peptide with Zn²⁺ and Cu²⁺ ions have been recently studied by our research group to obtain information on stoichiometry and structure of complex species formed throughout a wide pH range⁹. Moreover, calcitermin proved to adopt a helical conformation in membranes, and Zn²⁺ and

¹Department of Chemical, Pharmaceutical and Agricultural Sciences, University of Ferrara, L. Borsari 46, 44121 Ferrara, Italy. ²Faculty of Chemistry, University of Wrocław, F. Joliot-Curie 14, 50-383 Wrocław, Poland. ³Department of Environmental and Prevention Sciences, University of Ferrara, L. Borsari 46, 44121 Ferrara, Italy. ✉email: blldns@unife.it

Cu^{2+} ions are able to enhance its antimicrobial activity against *C. albicans* and common bacteria like *S. aureus* and *E. faecalis*^{9–11}.

In order to improve the microbicide activity of calcitermin, different strategies can be employed: (i) extending its life-time, i.e. its resistance to proteases; (ii) enhancing its sequestering ability towards the metal micronutrients (necessary for the survival and virulence of pathogens), thus hampering the microbe growth; (iii) changing the peptide charge and structure before and/or after the metal interaction^{12,13}. It is worth to note that three calcitermin His-to-Ala mutants – H9A, H11A and H13A, where one histidine residue is replaced with alanine—exhibit promising antimicrobial activity according to the estimated minimal inhibitory concentrations (MIC) in vitro⁹. These calcitermin mutants indeed represent an outstanding example of how different metal coordination modes (obtained by means of His-to-Ala substitution) result in significant changes of their antimicrobial properties. This type of information can be obtained through a detailed investigation on thermodynamics and coordination chemistry of the metal-peptide interaction, which can lay the foundations for a deeper insight into the way of action of metal chelating AMPs, in order to design new effective antibiotic therapies.

Considering the above results, this work is aimed at finding calcitermin derivatives where the peptide structure and, consequently, its physico-chemical properties are modified in order to achieve, first of all, a longer half-life and a lower proteolytic susceptibility, without losing its antimicrobial properties. Several strategies to improve the stability of peptides have been explored in the last forty years¹⁴. To increase the resistance towards exo-peptidases one common strategy is based on the chemical modification of one or both the peptide ends (e.g. by *N*-acylation, *C*-amidation, cyclization, binding to polyethyleneglycol)⁸. The degradation by endo-peptidases can be instead prevented by replacing one or more residues with non-proteinogenic amino acids which are normally not recognized by enzymes, like *D*-amino acids¹⁵, *N*-methyl- α -amino acids¹⁶, β - and γ - amino acids^{17–19}, α -alkylated amino acids²⁰, *N*-substituted glycines²¹.

Given the importance of the peptide termini in the degradation processes carried out by exopeptidases—enzymes that catalyze the cleavage of the terminal peptide bonds—we protected the amino- and carboxyl-termini of calcitermin by acetylation and amidation respectively²², obtaining the following derivatives: Ac-VAIALKAAHYHHTHKE (L1), Ac-VAIALKAAHYHHTHKE-NH₂ (L2) and VAIALKAAHYHHTHKE-NH₂ (L3). The terminal protection should confer higher proteolytic stability and preserve the principal metal binding site of calcitermin, corresponding to the histidine motif -HxHxH-. Moreover, the study of the protected peptides will elucidate the role of the terminal groups in calcitermin antimicrobial and metal-chelating properties. An in-depth investigation on the complex-formation equilibria of these derivatives with Zn^{2+} and Cu^{2+} ions, together with their stability and activity, will provide further information on their way of action.

Results and discussion

Under the experimental conditions here employed, only variously protonated mononuclear complexes, with metal/ligand stoichiometry of 1:1, have been detected by potentiometry and mass spectrometry. No precipitation has been observed over the explored pH range (2.5–10.5). The overall complex-formation constants ($\log\beta$) and corresponding acid dissociation constants ($\text{p}K_a$) are reported in Tables 1, 2 and Tables S1, S2, and the calculated species distribution diagrams for each system are shown in Figs. S1–S8. Spectroscopic results, including Vis absorption spectra, CD spectra and EPR spectra, recorded at different pH values, are shown in Figs. S9–S20.

Species	Ac-VAIALKAAHYHHTHKE (L1)			Ac-VAIALKAAHYHHTHKE-NH ₂ (L2)		
	$\log\beta$	$\text{p}K_a$	Coordination	$\log\beta$	$\text{p}K_a$	Coordination
[CuH ₂ L] ⁴⁺	18.21(3)	4.40	N _{im} , COO ⁻	23.06(4)	5.49	2N _{im}
[CuHL] ³⁺	13.81(2)	5.38	2N _{im} , COO ⁻	17.57(5)	6.30	3N _{im}
[CuL] ²⁺	8.43(2)	6.59	3N _{im}	11.27(7)	6.70	3N _{im} , N ⁻
[CuH ₁ L] ⁺	1.84(3)	6.88	3N _{im} , N ⁻	4.57(6)	9.44	2N _{im} , 2N ⁻
[CuH ₂ L] ⁻	-5.04(3)	-	2N _{im} , 2N ⁻	-4.87(9)	9.91	2N _{im} , 2N ⁻
[CuH ₃ L] ⁻	-	-	-	-14.78(7)	-	N _{im} , 3N ⁻
Species	VAIALKAAHYHHTHKE-NH ₂ (L3)					
	$\log\beta$	$\text{p}K_a$	Coordination			
[CuH ₅ L] ⁵⁺	51.38(2)	5.16	2N _{im}			
[CuH ₄ L] ⁴⁺	46.21(2)	6.21	3N _{im}			
[CuH ₃ L] ³⁺	40.00(3)	6.90	2N _{im} , NH ₂			
[CuH ₂ L] ²⁺	33.11(2)	7.75	2N _{im} , NH ₂ , N ⁻			
[CuHL] ⁺	25.36(3)	9.53	2N _{im} , 2N ⁻			
[CuL]	15.83(5)	10.01	2N _{im} , 2N ⁻			
[CuH ₁ L] ⁻	5.82(4)	-	N _{im} , 3N ⁻			
[CuH ₃ L] ³⁻	-15.03(9)	-	N _{im} , 3N ⁻			

Table 1. Equilibrium constants and proposed coordination modes for Cu^{2+} complexes at $T = 298$ K and $I = 0.1$ M (KCl). Values in parentheses are standard deviations on the last significant figure.

Species	Ac-VAIALKAAHYHTHKE (L1)			Ac-VAIALKAAHYHTHKE-NH ₂ (L2)		
	logβ	pK _a	Coordination	logβ	pK _a	Coordination
[ZnH ₂ L] ⁴⁺	–	–	–	20.29(6)	6.14	2N _{im}
[ZnHL] ³⁺	11.00(5)	5.80	2N _{im}	14.15(4)	7.63	3N _{im}
[ZnL] ²⁺	5.21(2)	7.33	3N _{im}	6.52(5)	8.93	3N _{im} , OH ⁻
[ZnH ₁ L] ⁺	-2.12(3)	–	3N _{im} , OH ⁻	-2.41(7)	9.44	3N _{im} , 2OH ⁻
[ZnH ₂ L]				-11.85(3)	–	3N _{im} , 2OH ⁻
Species	VAIALKAAHYHTHKE-NH ₂ (L3)					
	logβ	pK _a	Coordination			
[ZnH ₅ L] ⁵⁺	48.7(1)	5.6	2N _{im}			
[ZnH ₄ L] ⁴⁺	43.07(3)	7.32	3N _{im}			
[ZnH ₃ L] ³⁺	35.75(6)	7.69	3N _{im} , OH ⁻			
[ZnH ₂ L] ²⁺	28.06(4)	8.65	3N _{im} , OH ⁻			
[ZnHL] ⁺	19.40(5)	9.47	3N _{im} , 2OH ⁻			
[ZnL]	9.94(4)	–	3N _{im} , 2OH ⁻			
[ZnH ₂ L] ²⁻	-10.70(7)	–	3N _{im} , 2OH ⁻			

Table 2. Equilibrium constants and proposed coordination modes for Zn²⁺ complexes at *T* = 298 K and *I* = 0.1 M (KCl). Values in parentheses are standard deviations on the last significant figure.

Formation of copper complexes with L1, L2 and L3

ESI-MS results are reported in Table S4 and Figs. S21–S23: the only detected *m/z* signals correspond to equimolar Cu²⁺ complexes with different protonation states. Potassium and/or sodium adducts are also formed. The formation of copper complexes in solution begins around pH 3–3.5. The first detected species, however, display different coordination modes depending on the system.

L1 is the only ligand with the free carboxyl terminus, and its first formed species, [CuH₂L]⁴⁺, is likely characterized by a coordination mode (N_{im}, COO⁻). In this case, besides the histidine residue, one or both the carboxyl groups of *C*-terminal glutamic acid can participate in the complexation, forming a macrocycle. The wavelength of maximum absorption measured at pH 4, at least partly imputable to the species [CuH₂L]⁴⁺ (760 nm, Fig. S9), is in fair agreement with the expected value for a coordination (N_{im}, COO⁻)²³, taking into account that at this pH most of the copper is still present as a hexa-aquo complex. The complex [CuH₂L]⁴⁺ is rapidly substituted in solution by the species [CuHL]³⁺, where a second histidine interacts with the metal center (pK_a = 4.40) giving a (2N_{im}, COO⁻) complex (experimental λ_{max} = 655 nm, Fig. S9; predicted λ_{max} = 663 nm²³). In the case of amidated peptides (**L2** and **L3**), the stoichiometry of the complex species formed at the most acidic pH values ([CuH₂L]⁴⁺ and [CuH₅L]⁵⁺, respectively) suggests that two histidines are already deprotonated. In other words, the protection of the *C*-terminus likely favors the initial formation of a 2N complex where Cu²⁺ interacts with two imidazole groups of the histidine side chains. Indeed, the 2N species are predominant in solution in the pH range 4–5.5. EPR spectra registered at pH 5.5 confirm the presence of 2N complexes (**L1**: A_{||} = 174; g_{||} = 2.28; g_⊥ = 2.02; **L2**: A_{||} = 157; g_{||} = 2.31; g_⊥ = 2.02; **L3**: A_{||} = 163; g_{||} = 2.28; g_⊥ = 2.02; Table S3)²⁴. Increasing the pH value, the Cu²⁺ ion can displace the acidic proton from a third histidine, and it coordinates three imidazoles forming a (3N_{im}) species, which is prevalent in solution at around pH 6 in all the systems. The obtained wavelengths of maximum absorption at pH 6.0 range from λ_{max} = 626 nm to λ_{max} = 635 nm and agree with the proposed coordination mode (expected λ_{max} = 627 nm)²³.

In the alkaline pH range, we can distinguish two situations depending on the considered system. In the case of acetylated peptides, **L1** and **L2**, the next deprotonation step involves an amide group of the peptide backbone, while in **L3**, the free terminal amino group can deprotonate and interact with the metal ion. The EPR results confirm the formation of 4N species, since the spectra above pH 7 show the same superhyperfine structure and the following EPR parameters: A_{||} = 182–198; g_{||} = 2.20–2.21; g_⊥ = 2.02–2.05 (Table S3), that agree with the expected literature values²⁴.

Examining in details the systems **L1** and **L2**, starting from pH 5.5, we can observe the formation of [CuH₁L]⁺ (for **L1**) and [CuL]²⁺ (for **L2**) (Figs. S3, S4) with pK_a = 6.59 and 6.30, respectively. The experimental values of λ_{max} for solutions where these complexes reach their maximum of formation is 557 nm (Figs. S9, S12), exactly the value expected for a coordination (3N_{im}, N⁻)²³. Circular dichroism spectra recorded at pH above 6 (Figs. S10, S13) also show the appearance of intense signals in the visible spectral region, which can be attributed to the coordination of the amide nitrogen (it is closer to the chiral α-carbon of the peptide backbone and therefore can produce a stronger CD absorption when the metal binding occurs). Increasing the pH value the intensity of CD bands increases suggesting the binding of a second amide that replaces a histidine in the equatorial plane of the complex, forming a (2N_{im}, 2N⁻) species and increasing the square-planar character of the corresponding complexes, [CuH₂L] (for **L1**) and [CuH₁L]⁺ (for **L2**)^{25,26}. For Cu²⁺/L2 system, increasing the pH two further species were detected [CuH₂L] and [CuH₃L]⁻. The former one is obtained with a pK_a = 9.44, likely corresponding to the deprotonation of the phenolic group of tyrosine, which does not participate in the metal complexation, while the latter one is formed under the most alkaline conditions and can be ascribed to the displacement of a

third amide proton, giving rise to the ($N_{im}, 3N^-$) species ($\lambda_{max} = 525$ nm) (Fig. 1a). The employed experimental techniques however do not allow to establish which His residues or backbone amides mainly participate in the complex formation.

As mentioned above, **L3** behaves differently than the acetylated analogues. Close to neutral pH, we observe the formation of the $[CuH_3L]^{3+}$ species, which dominates around pH 6.5. The Vis spectra show a clear blue-shift between pH 5.5 (where $[CuH_4L]^{4+}$ complex is predominant) and pH 6.5, but the wavelength of maximum absorption does not drop below 600 nm, as expected for 4N-type Cu^{2+} complexes (*i.e.* with four equatorially bound nitrogen atoms). Therefore, it can be assumed that the increase of pH favors the coordination of the terminal amine that replaces an imidazole donor group in the metal coordination sphere (Fig. 1b). The prevailing complex at physiological pH is $[CuH_2L]^{2+}$: the wavelength of maximum absorption significantly decreases, and the value recorded at pH 7.5 (553 nm) is very close to both those expected for a coordination ($3N_{im}, N^-$) (557 nm) and ($2N_{im}, NH_2, N^-$) (549 nm). It cannot be excluded that both complexes are present in solution, or that it may exist a continuous and rapid “interconversion” between them, given the lability of the coordination bonds with the Cu^{2+} ion. Above pH 7.5, once again we observed the gradual coordination of three backbone amides, forming ($2N_{im}, 2N^-$) and ($N_{im}, 3N^-$) species, which dominate under alkaline conditions. The tyrosine and the two lysine residues simply lose their proton without participating in the complexation.

Formation of zinc complexes with **L1**, **L2** and **L3**

Only mononuclear zinc complexes have been identified under the employed experimental conditions. MS spectra confirm the presence of different Zn^{2+} complexes with various protonation states: $[ZnHL]^{3+}$ (**L1**, $m/z = 599.3$), $[ZnL]^{2+}$ (**L2**, $m/z = 898.4$), $[ZnH_3L]^{3+}$ (**L3**, $m/z = 584.6$) and $[ZnH_2L \cdot K]^{3+}$ (**L3**, $m/z = 597.3$) (Table S4). For all the systems, the stoichiometry of the first identified species indicates that only one histidine residue is protonated and therefore the Zn^{2+} ion should coordinate two imidazole nitrogens, with a geometry that can be reasonably assumed to be tetrahedral²⁸. The terminal Glu residue (or at least one of its carboxylate moieties in **L1**) can also bind the metal replacing a water molecule, as already reported for wild-type calcitermin⁹. When pH is increased, an acidic proton is released from the third histidine with a pK_a of 5.80 (**L1**), 6.14 (**L2**) and 5.6 (**L3**), forming the species ($3N_{im}$) where the third His can replace the carboxylate group (if coordinated) in the set of donor groups. A further deprotonation step leads to the formation of complexes $[ZnH_{-1}L]^+$ (**L1**, $pK_a = 7.33$), $[ZnL]^{2+}$ (**L2**, $pK_a = 7.63$) and $[ZnH_3L]^{3+}$ (**L3**, $pK_a = 7.32$). In these cases, the release of the proton is attributable to the ionization of a coordinated water molecule. Increasing the pH, the complex-formation pattern and the geometry of the formed complexes with the acetylated peptides, **L1** and **L2**, are practically the same, with the only difference that, in the case of **L2**, we observe the deprotonation of the Tyr residue ($pK_a = 9.44$) without metal coordination. The formed zinc species with **L1** and **L2** are most likely tetrahedral complexes with two or three coordinated histidines (Fig. 2), while water molecules saturate the coordination sphere. Instead, in the case of **L3**, after the formation of $[ZnH_3L]^{3+}$, we observe the mere deprotonation of the four basic sites of the ligand, in the order: the terminal amine ($pK_a = 7.69$), the phenolic oxygen of tyrosine ($pK_a = 9.47$), and the two ϵ -amino groups of lysines. In the end, above pH 9 and in the case of the amidated peptides, the formation of $[ZnHL]^+$ (for **L3**) and $[ZnH_{-1}L]^+$ (for **L2**) may be due to the release of an acidic proton from a second water molecule, which occupies a coordination position in a trigonal bipyramidal complex.

Comparison of metal chelating abilities

Competition diagrams (Fig. S24) allow to compare the overall capacity of the studied ligands to coordinate Zn^{2+} or Cu^{2+} ions. Although they can be used only for a qualitative comparison of the binding affinities, the stability of

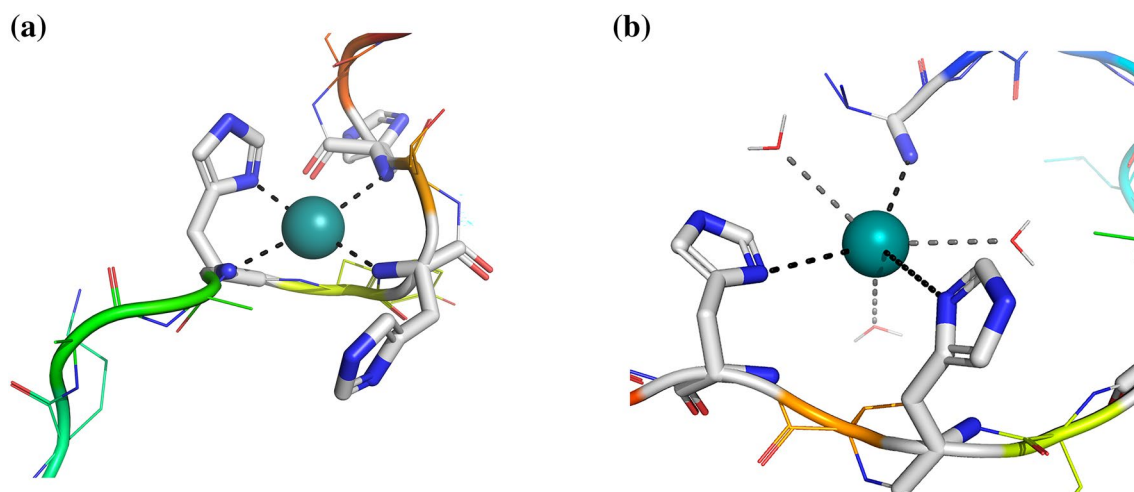


Figure 1. (a) Coordination hypothesis ($N_{im}, 3N^-$) for $[CuH_3L]^-$ species of peptide **L2**. (b) Coordination hypothesis ($2N_{im}, NH_2$) for the $[CuH_3L]^{3+}$ species of peptide **L3**. Molecular structure generated with PyMol²⁷.

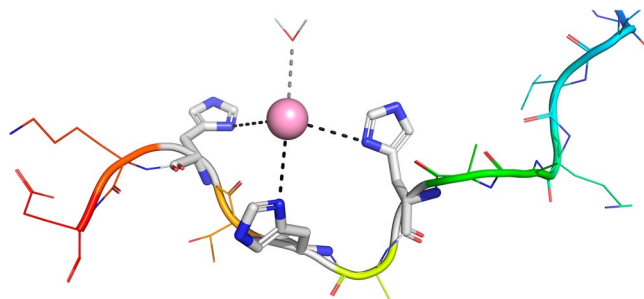


Figure 2. Coordination hypothesis for the $(3N_{im}) Zn^{2+}$ complexes. Molecular structure generated with PyMol²⁷.

the formed complexes in the entire explored pH range, regardless of stoichiometry and structure of the formed species, can be evaluated.

In Fig. S24a the affinity for copper of the wild-type calcitermin is compared to that of its protected derivatives. The metal chelating ability of WT and L1 is the same under acidic conditions. The presence of the terminal carboxylic group moderately enhances the stability of the formed complexes. Above pH 4.5, WT exhibits the best copper binding ability. Both the free terminal amine and carboxylate contribute to thermodynamically favour the formed complexes, thanks to the presence of a higher number of donor sites. On the other hand, the metal binding ability of the protected analogues above pH 5 is comparable. This is in accordance with the speciation models that indicate a similar coordination behaviour for these systems, with the progressive binding of the three histidines, followed by the terminal amino group and the backbone amides.

In the case of zinc (Fig. S24b), WT is a slightly better ligand in the entire pH range. The protected analogues behave similarly up to pH 6, after which the greater stability is shown by the complexes formed by the *N*-acetylated peptide, L1. This trend can confirm that the terminal amine is not involved in zinc complexation. On the contrary, the *C*-terminal carboxyl group seems to stabilize the formation of the complexes; suggesting that Glu residue takes part in the coordination by means of its side chain and/or terminal COOH, as in the case of WT⁹.

Peptide stability in plasma

The stability of the investigated peptides in human plasma is reported in Fig. 3a and is compared with the proteolytic susceptibility of wild-type calcitermin (WT). The concentration of all the peptides decreases with an approximately exponential decay and a half-life period ($t_{1/2}$) of about 20 min for L3, 68 min for L2 and more than two hours (135 min predicted with an exponential regression) in the case of L1. The degradation profile of L3 follows that of the native peptide, with a $t_{1/2}$ comparable to the value obtained for WT ($t_{1/2} = 18 \pm 3$ min). On the contrary the acetylated peptides, L1 and L2, showed an improved resistance to degradation, with L1 displaying the highest persistence in the human plasma. This result highlights the efficacy of the *N*-terminus protection as a general method to increase the resistance to proteolytic degradation of antimicrobial peptides⁸. The amidation of the *C*-terminus, instead, seems to affect less the resistance of calcitermin toward the activity of peptidases.

The effect of metal complex formation on the peptide stability has been evaluated for WT and L1—the least and most stable peptides, respectively. The complexation of Cu^{2+} and Zn^{2+} increases the half-life of WT from

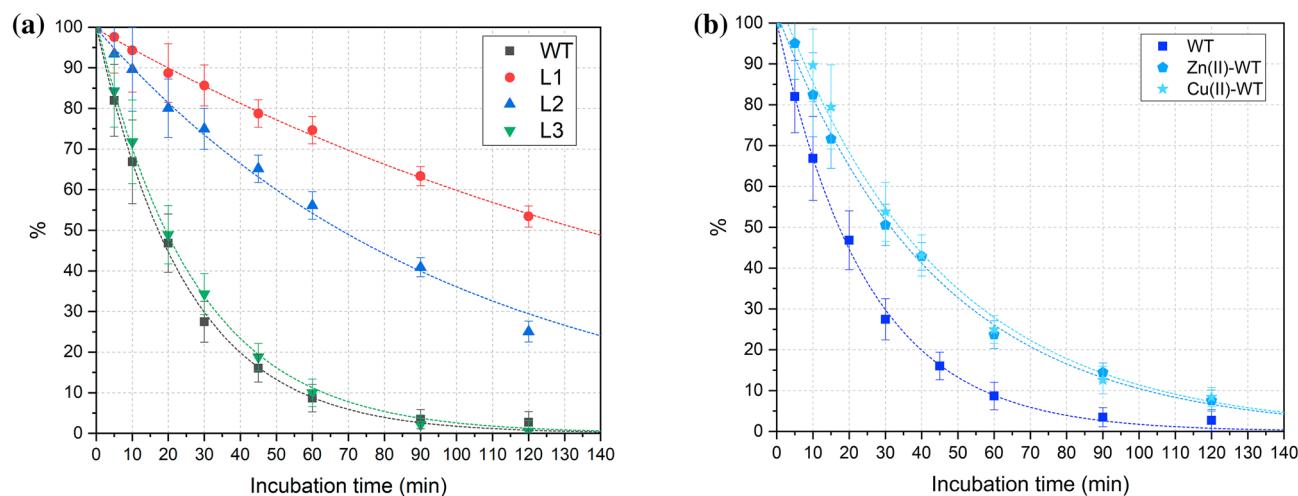


Figure 3. Stability in human plasma of wild-type calcitermin (WT) and its (a) *N*- and/or *C*-terminal protected analogues (L1, L2, L3); or (b) Zn^{2+} and Cu^{2+} complexes.

18 min to about 33 min (Fig. 3b), while the $t_{1/2}$ rises from 135 min to ≈ 150 min (Zn^{2+}) or ≈ 160 min (Cu^{2+}) in the case of **L1** (Fig. S25).

Antimicrobial activity

The antimicrobial activity of **WT** calcitermin and its protected derivatives (**L1**, **L2**, **L3**) was assessed on *C. albicans*, *S. aureus*, and *E. coli*, respectively representative of human pathogens of fungal and bacterial origin.

Regarding *C. albicans* (Fig. 4), the results showed a remarkable CFU reduction of the yeast in the presence of **WT** compared to untreated controls. The reduction was already evident after 3 h (Fig. 4A), with all used concentrations, despite a true dose-dependence was not observable (-67% , -67% , and -73% , for 0.032–0.064 and 0.128 mg/mL respectively, $p < 0.05$). A significant reduction was also observed with 0.128 mg/mL **WT** in the presence of ZnCl_2 (-49% , $p < 0.05$), whereas no significant reduction was observed for the Cu^{2+}/WT complex. After 24 h of contact, the reduction was maintained and remarkably increased by ZnCl_2 presence, especially at 0.128 mg/mL (-96% , $p < 0.0001$) (Fig. 4B). Instead, at 3 h, the **L1** derivative exhibited some antifungal action only at 0.128 mg/mL (Fig. 4C). At 24 h, limited yet significant CFU reduction was observed with **L1** alone (-18% , -17% , and -23% , for 0.032, 0.064, and 0.128 mg/mL, respectively; $p < 0.05$), and increased activity was detected with the addition of ZnCl_2 (-26% and -88% , for 0.064 mg/mL and 0.128 mg/mL, $p < 0.05$ and $p < 0.001$, respectively). Some CFU decrease was also observed with **L1** + CuCl_2 (-12% , -28% and -34% for 0.032, 0.064, and 0.128 mg/mL, respectively; $p < 0.05$) (Fig. 4C,D). Similarly, at 3 h, the **L2** derivative was significantly active only at 0.128 mg/mL in the presence of ZnCl_2 (-74% , $p < 0.01$), while at 24 h a significant CFU reduction was observed at 0.064 and 0.128 mg/mL plus ZnCl_2 (respectively -46% , $p < 0.0001$; and -97% , $p < 0.0001$) and plus CuCl_2 (-17% and -23% , respectively; $p < 0.01$) (Fig. 4E,F). Comparable results were observed for **L3**, which at 3 h was active only at 0.128 mg/mL in the presence of ZnCl_2 (-51% , $p < 0.01$), and at 24 h exhibited antifungal activity at 0.064 and 0.128 mg/mL in the presence of ZnCl_2 (respectively -37% , $p < 0.05$; and -76% , $p < 0.01$) (Fig. 4G,H). ZnCl_2 alone, included as a control, exhibited a significant antifungal activity in all performed assays, reducing *C. albicans* CFU number up to 64.9% at 3 h and to 94% at 24 h ($p < 0.0001$). By contrast, negligible or no CFU reduction was observed in all conditions with CuCl_2 alone, which significantly reduced *C. albicans* CFU number only at 24 h, in one out of the total performed assays (Table S5).

Summarizing, the results on *C. albicans* confirmed the antifungal activity of **WT** calcitermin, even at low concentrations, at both 3 and 24 h. The **WT**/zinc complex was quite effective against *C. albicans* at 24 h, at 0.128 mg/mL, although only a slightly lower activity was found for ZnCl_2 itself at the same concentration. On the other hand, no activity was shown by CuCl_2 alone and its presence did not significantly affect the **WT** activity, although Cu^{2+} can form stable complexes with calcitermin even at pH 5.4. Of note, previous studies showed that both Zn^{2+} and Cu^{2+} ions possess antifungal activity per se at concentrations consistent with those used in our study, showing similar minimal inhibitory concentrations, although Zn^{2+} was generally proven to be more effective compared to Cu^{2+} ^{29–31}. Our results confirmed the Zn^{2+} anti-*C. albicans* activity, whereas a marked antifungal activity by Cu^{2+} ion was not evidenced. This might be due to: the different type of assay performed in our study compared to those previously reported; the different metal ion formulations tested (Zn/Cu chloride vs. Zn/Cu oxide), the absence in our study of a nanoparticle delivery system^{32,33}; the suboptimal concentrations of ions used in our assays, which may have induced some yeast tolerance to metal ions. Further studies would be needed to address these points. The amidation of the carboxyl terminal (peptides **L2** and **L3**) did not improve the antifungal activity of **WT**, also in the presence of zinc. Some effect due to acetylation of the *N*-terminus of calcitermin (**L1** and **L2** peptides) was observed in the presence of CuCl_2 , after 24 h; in particular, Cu^{2+} complexes with a concentration of 0.128 mg/mL were significantly more active than both the corresponding controls and the calcitermin complexes.

The antimicrobial action of calcitermin and its derivatives was also tested on bacteria, including the Gram-negative bacillus *E. coli* and the Gram-positive coccus *S. aureus*. Regarding *E. coli*, the results showed that **WT** was active essentially in the presence of ZnCl_2 or CuCl_2 (Fig. 5A,B). At 3 h, the CFU number decreased to -38% ($p < 0.05$), -55% ($p < 0.01$), and -91% ($p < 0.001$) with respect to controls, using 0.032, 0.064, and 0.128 mg/mL of peptide + ZnCl_2 , respectively. With the addition of CuCl_2 , the CFU decrease corresponded to -38% ($p < 0.01$), -56% ($p < 0.05$), and -91% ($p < 0.001$) for 0.032, 0.064, and 0.128 mg/mL of peptide, respectively. At 24 h, no significant CFU reduction was observed with **WT** with or without ZnCl_2 , whereas a -82% decrease of CFU number was detected with 0.128 mg/mL of calcitermin in the presence of CuCl_2 ($p < 0.0001$).

Differently from **WT**, the **L1** derivative induced a dose-dependent CFU decrease at 3 h (-28% , -39% , and -40% , for 0.032, 0.064, and 0.128 mg/mL, respectively; $p < 0.05$). The reduction was increased in the presence of ZnCl_2 (-67% , -81% , and -96% , respectively; $p < 0.001$), and CuCl_2 (-65% , -63% , and -85% for 0.032, 0.064, and 0.128 mg/mL, respectively; $p < 0.01$). At 24 h, **L1** was active only at 0.128 mg/mL, alone (-19% , $p < 0.05$) or in the presence of CuCl_2 , which significantly increased **L1** action (-67% and -90% for 0.064 and 0.128 mg/mL, respectively; $p < 0.001$) (Fig. 5C,D).

A similar trend was observed for **L2**, which at 3 h reduced *E. coli* CFUs only in the presence of ZnCl_2 (-64% , -76% , and -96% at 0.032, 0.064 and 0.128 mg/mL, respectively; $p < 0.001$) or CuCl_2 (-55% , -65% , and -82% , respectively; $p < 0.01$). At 24 h, no significant CFU reduction was observed except for 0.032 and 0.064 mg/mL in the presence of ZnCl_2 (Fig. 5E,F). The activity of the **L3** derivative was essentially detectable only at 3 h in the presence of ZnCl_2 and CuCl_2 , inducing a significant CFU decrease at 0.032, 0.064 and 0.128 mg/mL (for ZnCl_2 , -58% , -79% , and -94% , respectively, $p < 0.001$; for CuCl_2 , -51% , -81% , and -82% , respectively, $p < 0.001$). After 24 h, no significant reduction was observed at any **L3** concentration, except for 0.128 mg/mL in the presence of CuCl_2 (-41% , $p < 0.01$) (Fig. 5G,H).

As also observed in the antifungal assays, ZnCl_2 exhibited an anti-*E. coli* activity per se, reducing the CFU number up to -95% at 3 h ($p < 0.0001$), although it was not anymore active at 24 h, showing a -30% reduction

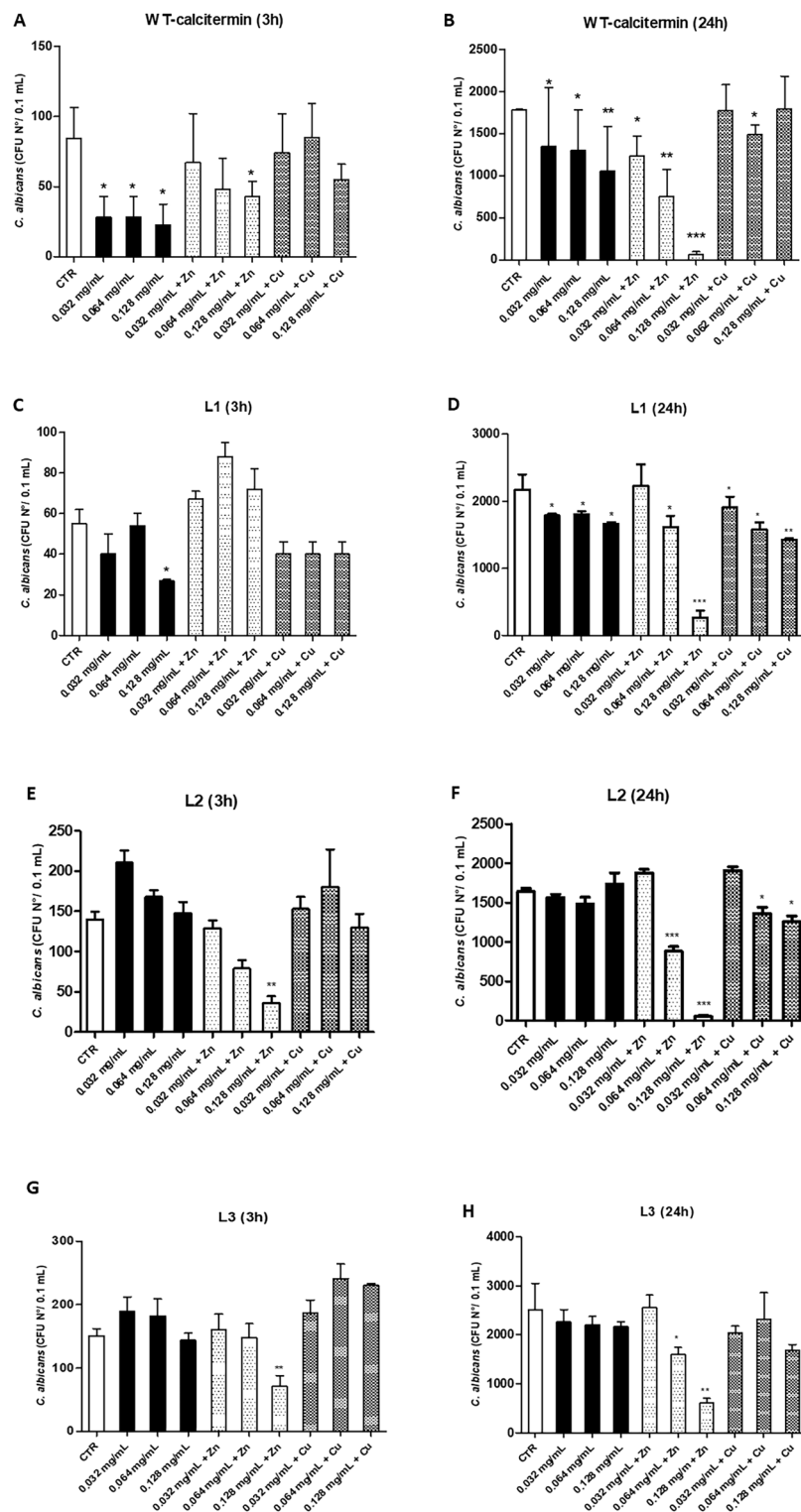


Figure 4. In vitro antifungal activity of WT and L1, L2, L3 derivatives. All assays were performed in the presence or absence of $ZnCl_2$ or $CuCl_2$ in aqueous buffer (5.4 pH). (A,B) WT-calcitermin action at 3 and 24 h-incubation; (C,D) L1 action at 3 and 24 h-incubation; (E,F) L2 action at 3 and 24 h-incubation; (G,H) L3 action at 3 and 24 h-incubation. Results are expressed as mean value of CFUs \pm SD obtained in triplicate samples from two independent experiments; * $p \leq 0.05$; ** $p \leq 0.01$; *** $p \leq 0.001$.

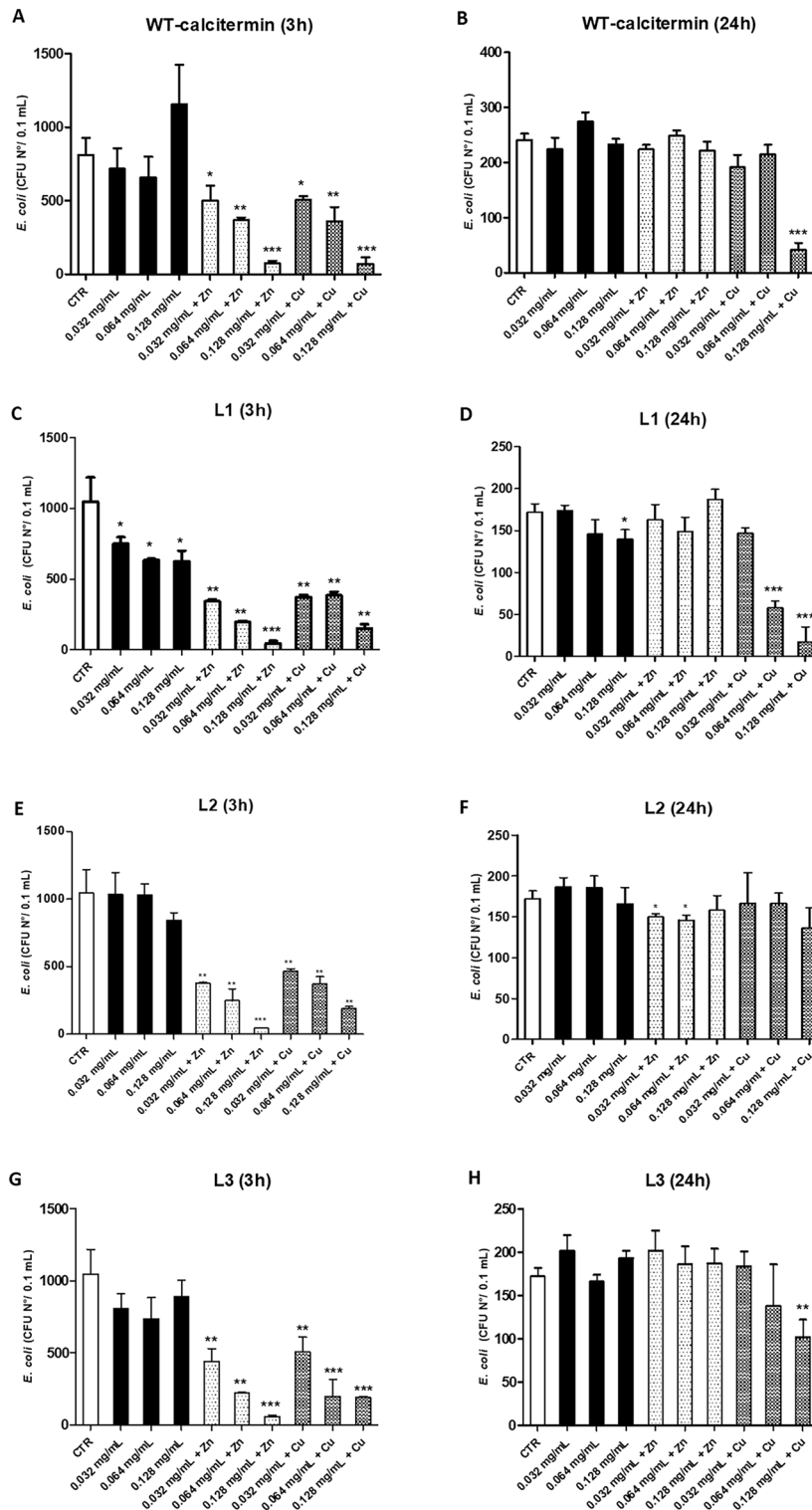


Figure 5. In vitro anti-*E. coli* activity of WT and L1, L2, L3 derivatives. All assays were performed in the presence or absence of ZnCl₂ or CuCl₂ in aqueous buffer (5.4 pH). (A,B) WT-calcitermin action at 3 and 24 h-incubation; (C,D) L1 action at 3 and 24 h-incubation; (E,F) L2 action at 3 and 24 h-incubation; (G,H) L3 action at 3 and 24 h-incubation. Results are expressed as mean value of CFUs ± SD obtained in triplicate samples from two independent experiments; *p ≤ 0.05; **p ≤ 0.01; ***p ≤ 0.001.

only in one of the performed assays ($p < 0.05$). Also CuCl_2 displayed a high antibacterial activity, inducing an up to 96% reduction at both 3 and 24 h of incubation ($p < 0.0001$) (Table S6). In conclusion, only the derivative **L1** showed a significant anti-*E. coli* activity in the absence of metals, especially after 3 h. Interestingly, **L1** was also the least sensitive peptide of the series towards the proteolytic enzymes. Copper and zinc exhibited antimicrobial activity against *E. coli* at 3 h, both in their free and complexed form; this behaviour was very similar for all peptides, regardless of the protection of the terminals. However, at 24 h, only copper (and its complexes) showed some activity, especially in the case of **L1**, whose complexes with Cu^{2+} were already active at the concentration of 0.064 mg/ml.

Regarding *S. aureus*, the assays were performed only at 3 h, since at 24 h of incubation in aqueous buffer at pH 5.4 no viable bacteria were detectable even in untreated controls. At 3 h, the data showed that **WT** was significantly active only at 0.128 mg/mL in the presence of ZnCl_2 (−41%, $p < 0.05$) (Fig. 6A).

Similarly, both **L1** and **L2** derivatives induced a significant CFU decrease only at 0.128 mg/mL in presence of ZnCl_2 (−46%, $p < 0.05$; −54%, $p < 0.01$, respectively for **L1** and **L2**) (Fig. 6B,C). **L3** action was instead more evident, inducing a CFU decrease corresponding to −28% ($p = \text{n.s.}$), −43% ($p < 0.05$), and −49% ($p < 0.05$) at 0.032, 0.064, and 0.128 mg/mL concentration, respectively. Moreover, the action of 0.128 mg/mL of **L3** was increased by the addition of ZnCl_2 (−73% CFU decrease, $p < 0.001$) (Fig. 6D), and by the presence of CuCl_2 (−47%, $p < 0.01$) (Fig. 6).

Likewise, ZnCl_2 alone showed a clear antimicrobial activity toward *S. aureus*, inducing an up to 77% CFU reduction, compared to controls (Table S7). Regarding *S. aureus*, in conclusion, **WT** calcitermin showed no effect, but a significant antimicrobial activity was observed for **L3**. Zn^{2+} complexes of all peptides were active at higher concentrations, especially when the terminals were protected. Among the Cu^{2+} complexes, only the one with **L3**

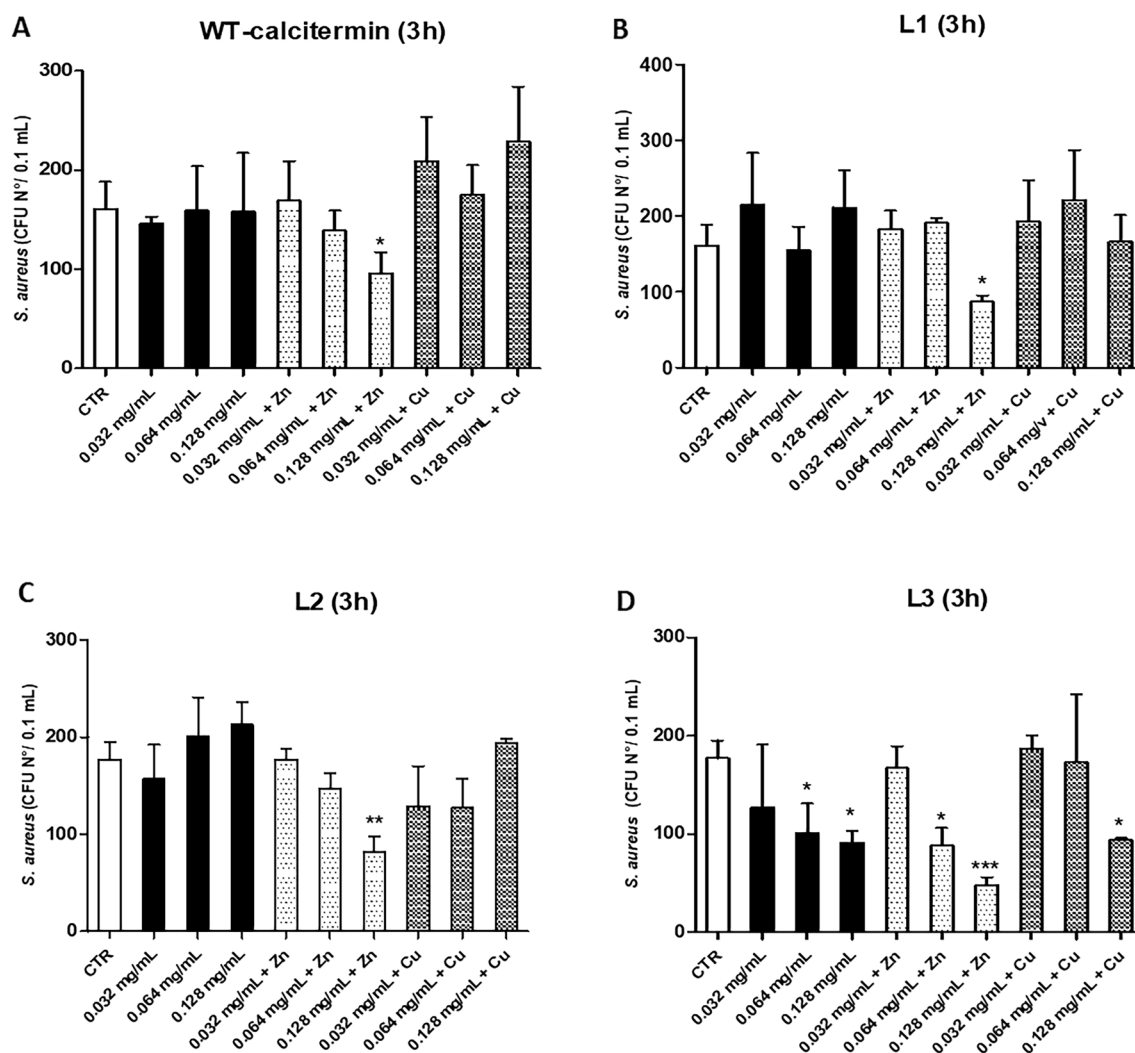


Figure 6. In vitro anti-*S. aureus* activity of WT and L1, L2, L3 derivatives. All assays were performed for 3 h-incubation time in the presence or absence of ZnCl_2 or CuCl_2 in aqueous buffer (pH 5.4). (A) WT-calcitermin action; (B) L1 action; (C) L2 action; (D) L3 action. Results are expressed as mean value of CFUs \pm SD obtained in triplicate samples from two independent experiments; * $p \leq 0.05$; ** $p \leq 0.01$; *** $p \leq 0.001$.

showed a detectable action, at a concentration of 0.128 mg/ml, although this was comparable to that shown by the same peptide in the absence of metals.

Concluding remarks

Although calcitermin and its antimicrobial activity have been known for over twenty years, this peptide is still sparsely studied as a potential new drug. The studies of Cole and coworkers¹⁰ first showed that bivalent endogenous metals, such as zinc and copper, can modulate the antimicrobial activity of calcitermin; later on, our research group investigated its metal binding properties. Then, a systematic study on calcitermin derivatives has begun, modifying the amino acid sequence in an opportune manner, with a view to improving interaction with cell membranes, to increasing stability towards proteolytic enzymes and/or to improving the sequestering ability towards metal ions to promote nutritional immunity. The encouraging previous results have led us to study the new calcitermin derivatives reported in this paper, where the native peptide has been protected at one or both of its termini. This is one of the ways, already known in the literature, to increase the resistance to proteolytic degradation of a peptide^{34–37}. However, since any variation in the structure of the peptide can affect both its ability to form metal complexes and its antimicrobial properties, we have carried out a thorough study, both from the chemical and microbiological point of view, to shed light on the behaviour of the modified peptides. The formation of metal complexes with calcitermin is driven by the presence of its three histidine residues. This coordination site is preserved in all peptides studied here, and stable complexes with all ligands have always been observed. According to Pearson's classification, in fact, the imidazole side chain of histidine is a good binding site (borderline basic character) for Cu^{2+} and Zn^{2+} ions (borderline Lewis acids)³⁸ and, on the basis of their electronic configuration, the Irving-Williams series also predicts a higher binding affinity for Cu^{2+} than Zn^{2+} ³⁹.

The metal coordination did not affect the peptide structure, and for all the systems a prevalence of random coil conformation was observed (Figs. S16–S18). However, the contribution to the complex-formation by the amino and carboxyl termini, although secondary, is evident: both with copper and zinc, the most stable complexes are always those formed by the native calcitermin, throughout the explored pH range. Noteworthy, the metal complexed forms of the studied peptides display higher resistance to degradation. Indeed, the formation of both copper and zinc complexes with calcitermin almost doubled its half-life in human plasma, suggesting that the interaction with metal ions can be a fruitful strategy to increase the peptide stability in biological fluids. Whether this correlates with the slightly better antimicrobial activity of the studied metal complexes is not easy to judge, and further investigation is required. Similarly, it is not straightforward to link the antimicrobial activity of the studied peptides with their stability in plasma.

Acetylation of the *N*-terminal confers a much longer half-life with respect to peptides with free amino terminus. This is an important indication for the design of calcitermin derivatives (as well as other AMP derivatives)^{35–37} that may persist in the body long enough to perform their microbicidal action. Indeed, the study of peptide degradation will be deepened trying to identify the responsible enzymes and the most vulnerable peptide bonds, also extending the investigation to other biological fluids, such as saliva and gastric juices. Moreover, a preliminary investigation on peptide interaction with albumin (one of the major proteins in plasma) has been carried out to evaluate the protein-peptide binding, which may affect the decrease of peptide concentration detected after incubation in plasma. We observed a variation in the α -helical content of albumin structure when the studied peptides are added to the solution (Fig. S26). The mechanism and effect of such interaction will require further specific investigations; however, all the investigated peptides, even in their metal complexed form, behave in the same way and decrease the same extent the α -helix structure of the protein. Therefore, the interaction with albumin does not affect the relative stability of calcitermin and its derivative systems.

Lastly, although the new calcitermin derivatives studied here were not particularly promising as commercial antimicrobials against fungi such as *C. albicans* or against Gram-positive or Gram-negative bacteria, encouraging results have been obtained for their metal (especially Zn^{2+}) complexes. The investigation will be therefore extended to other derivatives, other microorganisms and other experimental conditions. In conclusion, calcitermin and its derivatives remain a promising class of peptides of great interest as new generation of metal-enhanced antimicrobials.

Methods

Potentiometry

Stability constants for proton and metal complexes were obtained from pH-metric titration curves registered at $T = 298$ K and ionic strength 0.1 M (KCl). The potentiometric apparatus was previously described⁴⁰. Solutions were titrated with 0.1 M carbonate-free KOH. The electrode was daily calibrated for hydrogen ion concentration by titrating HNO_3 with the standard base solution, under the same experimental conditions as above. The asymmetry potential and the slope of the electrode couple were computed by means of SUPERQUAD⁴¹ and Glee⁴² programs. The purities and exact concentrations of the ligand solutions were determined by the Gran method⁴³. The HYPERQUAD⁴⁴ program was employed for the overall formation constant (β) calculations, referred to the following equilibrium equation: $\text{pM} + \text{qL} + \text{rH} \rightleftharpoons \text{M}_p\text{L}_q\text{H}_r$ (charges omitted; p is 0 in the case of ligand protonation; r can be negative). The computed standard deviations (referring to random errors only) were given by the program itself and are shown in parentheses as uncertainties on the last significant figure. Hydrolysis constants for metal ions were taken from the literature^{45,46}. The distribution and competition diagrams were computed using the HYSS program⁴⁷.

Mass spectrometry

High-resolution mass spectra were obtained on the LCMS-9030 qTOF Shimadzu (Shimadzu, Kyoto, Japan), equipped with a standard ESI source and the Nexera X2 system. The instrumental parameters were as follows:

positive ion mode, scan range m/z 100–3000, dry gas nitrogen, temperature 170 °C, and ion energy 5 eV. The capillary voltage was optimized to the highest S/N ratio and it was 4500 V. The small changes in voltage (± 500 V) did not significantly affect the optimized spectra. The samples ($[L]_{\text{tot}} = 1 \cdot 10^{-4}$ M and M:L molar ratio = 1:1) were prepared in a 1:1 methanol–water mixture at pH 5.2 and 7.4. They were directly infused at a flow rate of 3 $\mu\text{l}/\text{min}$. The instrument was externally calibrated with a Tunemix™ mixture (Bruker Daltonik, Germany) in quadratic regression mode. Data were processed using the Bruker Compass DataAnalysis 4.2 program. The mass accuracy for the calibration was > 5 ppm, enabling together with the true isotopic pattern (using SigmaFit) an unambiguous confirmation of the elemental composition of the obtained complex.

Spectroscopic measurements

The absorption spectra of Cu^{2+} containing solutions were recorded on a Varian Cary50 Probe spectrophotometer, in the range 350–900 nm, using a quartz cuvette with an optical path of 1 cm. To describe the species present in solution, the observed wavelength of maximum absorption at a given pH was compared with the expected λ_{max} value obtained from literature^{23,48–50}. Circular dichroism (CD) spectra were recorded on a Jasco J-1500 spectropolarimeter in the 180–800 nm range, using a quartz cuvette with an optical path of 1 cm in the visible and near-UV range, and 0.01 cm in the 180–250 nm range. Electron paramagnetic resonance (EPR) spectra were recorded in liquid nitrogen on a Bruker ELEXSYS E500 CW-EPR spectrometer at X-band frequency (9.5 GHz) and equipped with an ER 036TM NMR teslameter and an E41 FC frequency counter. Ethylene glycol (30%) was used as a cryoprotectant. The EPR parameters were analyzed by computer simulation of the experimental spectra using WIN-EPR SIMFONIA software, version 1.2 (Bruker, Billerica, MA, USA).

Peptide stability in plasma

The persistence of calcitermin and its analogues and metal complexes in human plasma has been studied in vitro by means of the following procedure⁵¹. Each peptide ($C = 1 \cdot 10^{-4}$ M) and metal complex (metal:ligand ratio 1:1) was incubated in a sample containing 1 ml of human plasma (obtained as a pool of 40 individuals from the University Hospital of Ferrara) and 1 ml of ammonium acetate buffer (pH 7.4) at 37 °C. L-phenylalaninol is added as internal standard. At regular time intervals, 200 μl aliquots were taken and enzymatic reaction was blocked by adding 300 μl of HClO_4 0.5 M. The sample was then centrifugated for 6 min at $14,000 \times g$. The supernatant was then filtered and analysed by HPLC. The analytical column was an Agilent Poroshell 120 SB-C18 (4.6×100 mm, 2.7 μm , pore size 120 Å). Flow rate = 0.5 ml/min, mobile phase $\text{H}_2\text{O} + 0.1\%$ v/v TFA, linear gradient from 0 to 60% of acetonitrile + 0.1% v/v TFA over 30 min for the elution of peptides, temperature 25 °C, detection wavelength 210 nm. The results on calcitermin are the mean of three independent measurements while only one test was performed with the three protected peptides; in the latter cases, the errors have been estimated on the basis of those obtained for the wild-type calcitermin. Informed consent was obtained from all subjects and/or their legal guardian(s) prior to the donation of blood samples. All experimental protocols were approved by the National Research and Research Transversal Processes boards at University of Ferrara. All methods were carried out in accordance with relevant guidelines and regulations.

Biological tests

The potential antimicrobial activity of wild-type calcitermin and N- and C- terminally protected derivatives was investigated by using the yeast *C. albicans* (ATCC 10231), the Gram-positive *S. aureus* (ATCC 25293), and the Gram-negative *E. coli* (ATCC 25922) (all from American Type Culture Collection, ATCC, Thermo Scientific, Milan, Italy). All microbes were grown at 37 °C in Tryptic Soy Broth (TSB; Biolife, Milan, Italy) or Tryptic Soy Agar plates (TSA, Biolife, Milan, Italy). Peptides were tested at a final concentration $C = 0.128, 0.064, 0.032$ mg/mL, in the presence or absence of ZnCl_2 or CuCl_2 , at a M:L molar ratio 0.9:1. Briefly, all the microbes were expanded in TSB at 37 °C under agitation for 12 h and then sub-cultured by 1:10 dilution in TSB under the same conditions until reaching $\text{OD}_{600\text{nm}} = 0.3–0.4$, as measured by spectrophotometric reading using a GENESYS 10S UV–Vis spectrophotometer (Thermo Scientific, Milan, Italy), corresponding to $0.9–1.2 \times 10^7$ colony forming units (CFU) per mL, $1.5–2 \times 10^8$ CFU/mL and $2.4–3.2 \times 10^8$ CFU/mL, for *C. albicans*, *S. aureus* and *E. coli* respectively. The cultures were then centrifuged at 4500 rpm for 10 min in a SL 8 centrifuge (TX-150 Rotor) (Thermo Scientific, Milan, Italy), and the cellular pellets were washed with PBS pH 5.4. Pelletized cultures were then suspended in 10 mL of PBS pH 5.4, then the suspensions were diluted to a final concentration of 10^4 CFU/mL. Aliquots of 100 μl (corresponding to 10^3 CFU) were seeded in each well of a 96-wells plate. 3 μl of TSB at pH 5.4 were added to each well to obtain a final 1.5% TSB concentration in the culture medium. Peptides were serially diluted in PBS pH 5.4 to $C = 0.257, 0.128, \text{ and } 0.064$ mg/mL. ZnCl_2 and CuCl_2 solutions were added where requested to obtain a M:L ratio 0.9:1. 100 μl of the prepared peptides $\pm \text{ZnCl}_2/\text{CuCl}_2$ solutions were then added to each well, obtaining the final 0.128, 0.064 and 0.032 mg/mL peptide concentrations in a total 0.2 mL volume. PBS alone and PBS + $\text{ZnCl}_2/\text{CuCl}_2$ solutions were included as controls. The plates were incubated at 37 °C on a platform rocker with slow stirring for 3 and 24 h. At the end of the incubation times, 100 μl aliquots were taken from each sample and diluted in PBS pH 5.4 to be seeded on TSA plates. Specifically, aliquots were diluted 1:10 at 3 h, and 1:200, 1:100,000 and 1:10 at 24 h, for *C. albicans*, *E. coli*, and *S. aureus* respectively. After incubation for 24 h at 37 °C, grown CFUs were enumerated. Samples were assayed in triplicate in two independent experiments. Student's *t*-test was used for the evaluation of significance in biological tests; a *p* value ≤ 0.05 was considered significant.

Data availability

The datasets used in the current study is available from the corresponding author upon request.

Received: 4 August 2023; Accepted: 19 October 2023

Published online: 25 October 2023

References

- Steckbeck, J. D., Deslouches, B. & Montelaro, R. C. Antimicrobial peptides: New drugs for bad bugs?. *Expert Opin. Biol. Ther.* **14**, 11–14. <https://doi.org/10.1517/14712598.2013.844227> (2014).
- Malanovic, N. & Lohner, K. Antimicrobial peptides targeting gram-positive bacteria. *Pharmaceuticals (Basel)* **9**, 59. <https://doi.org/10.3390/ph9030059> (2016).
- Vishnepolsky, B. *et al.* De novo design and in vitro testing of antimicrobial peptides against gram-negative bacteria. *Pharmaceuticals (Basel)* **12**, 82. <https://doi.org/10.3390/ph12020082> (2019).
- Lugardon, K. *et al.* Antibacterial and antifungal activities of vasostatin-1, the N-terminal fragment of chromogranin A. *J. Biol. Chem.* **275**, 10745–10753. <https://doi.org/10.1074/jbc.275.15.10745> (2000).
- Chernysh, S. *et al.* Antiviral and antitumor peptides from insects. *Proc. Natl. Acad. Sci. U. S. A.* **99**, 12628. <https://doi.org/10.1073/pnas.192301899> (2002).
- Wang, G., Li, X. & Wang, Z. APD3: The antimicrobial peptide database as a tool for research and education. *Nucleic Acids Res.* **44**, 1087–1093. <https://doi.org/10.1093/nar/gkv1278> (2016).
- Gülseren, İ & Vahapoglu, B. The stability of food bioactive peptides in blood: An overview. *Int. J. Pept. Res. Ther.* **28**, 2. <https://doi.org/10.1007/s10989-021-10321-w> (2021).
- Bellotti, D. & Remelli, M. Lights and shadows on the therapeutic use of antimicrobial peptides. *Molecules* **27**, 4584. <https://doi.org/10.3390/molecules27144584> (2022).
- Bellotti, D. *et al.* Bioinorganic chemistry of calcitermin—The picklock of its antimicrobial activity. *Dalton Trans.* **48**, 13740–13752. <https://doi.org/10.1039/c9dt02869b> (2019).
- Cole, A. M. *et al.* Calcitermin, a novel antimicrobial peptide isolated from human airway secretions. *FEBS Lett.* **504**, 5–10. [https://doi.org/10.1016/S0014-5793\(01\)02731-4](https://doi.org/10.1016/S0014-5793(01)02731-4) (2001).
- Bellotti, D. *et al.* Calcitermin-loaded smart gels activity against *Candida albicans*: A preliminary in vitro study. *Gels* **9**, 165 (2023).
- Jiang, H. *et al.* A branched tripeptide with an anion-binding motif as a new delivery carrier for efficient gene transfection. *ChemBioChem* **20**, 1410–1416. <https://doi.org/10.1002/cbic.201800728> (2019).
- Alexander, J. L., Thompson, Z. & Cowan, J. A. Antimicrobial metallopeptides. *ACS Chem. Biol.* **13**, 844–853. <https://doi.org/10.1021/acscchembio.7b00989> (2018).
- Lenci, E. & Trabocchi, A. Peptidomimetic toolbox for drug discovery. *Chem. Soc. Rev.* **49**, 3262–3277. <https://doi.org/10.1039/D0CS00102C> (2020).
- Mutter, M. & Tuchscherer, G. Non-native architectures in protein design and mimicry. *Cell. Mol. Life Sci.* **53**, 851–863. <https://doi.org/10.1007/s000180050105> (1997).
- Sandberg, B. E. B., Lee, C. M., Hanley, M. R. & Iversen, L. L. Synthesis and biological properties of enzyme-resistant analogs of substance-P. *Eur. J. Biochem.* **114**, 329–337. <https://doi.org/10.1111/j.1432-1033.1981.tb05152.x> (1981).
- Porter, E. A., Weisblum, B. & Gellman, S. H. Mimicry of host-defense peptides by unnatural oligomers: Antimicrobial β -peptides. *J. Am. Chem. Soc.* **124**, 7324–7330. <https://doi.org/10.1021/ja0260871> (2002).
- Cabrele, C., Martinek, T. A., Reiser, O. & Berlicki, E. Peptides containing β -amino acid patterns: Challenges and successes in medicinal chemistry. *J. Med. Chem.* **57**, 9718–9739. <https://doi.org/10.1021/jm5010896> (2014).
- Robinson, J. A. Folded synthetic peptides and other molecules targeting outer membrane protein complexes in gram-negative bacteria. *Front. Chem.* **7**, 1–11. <https://doi.org/10.3389/fchem.2019.00045> (2019).
- Degenkolb, T. & Brückner, H. Peptaibiotics: Towards a myriad of bioactive peptides containing Ca-dialkylamino acids?. *Chem. Biodivers.* **5**, 1817–1843. <https://doi.org/10.1002/cbdv.200890171> (2008).
- Dancs, Á. *et al.* Tuning the coordination properties of multi-histidine peptides by using a tripodal scaffold: Solution chemical study and catechol oxidase mimicking. *NJCh* **41**, 808–823. <https://doi.org/10.1039/c6nj03126a> (2017).
- Shi, S. M. & Di, L. In *Peptide Therapeutics: Fundamentals of Design, Development, and Delivery* (ed. Jois, S. D.) 163–182 (Springer International Publishing, 2022).
- Sigel, H. & Martin, R. B. Coordinating properties of the amide bond. Stability and structure of metal ion complexes of peptides and related ligands. *Chem. Rev.* **82**, 385–426. <https://doi.org/10.1021/cr00050a003> (1982).
- Peisach, J. & Blumberg, W. E. Structural implications derived from the analysis of electron paramagnetic resonance spectra of natural and artificial copper proteins. *Arch. Biochem. Biophys.* **165**, 691–708. [https://doi.org/10.1016/0003-9861\(74\)90298-7](https://doi.org/10.1016/0003-9861(74)90298-7) (1974).
- Stanyon, H. F. *et al.* Developing predictive rules for coordination geometry from visible circular dichroism of copper(II) and nickel(II) ions in histidine and amide main-chain complexes. *FEBS J.* **281**, 3945–3954. <https://doi.org/10.1111/febs.12934> (2014).
- Daniele, P. G., Prenesti, E. & Ostacoli, G. Ultraviolet–circular dichroism spectra for structural analysis of copper(II) complexes with aliphatic and aromatic ligands in aqueous solution. *Dalton Trans.* **15**, 3269–3275 (1996).
- The PyMOL Molecular Graphics System, V. r. p., Schrödinger, LLC.
- Alberts, I. L., Nadassy, K. & Wodak, S. J. Analysis of zinc binding sites in protein crystal structures. *Protein Sci.* **7**, 1700–1716. <https://doi.org/10.1002/pro.5560070805> (1998).
- Djearmane, S. *et al.* Antifungal properties of zinc oxide nanoparticles on *Candida albicans*. *Coatings* **12**, 1864 (2022).
- Pasquet, J. *et al.* The contribution of zinc ions to the antimicrobial activity of zinc oxide. *Colloids Surf. Physicochem. Eng. Aspects* **457**, 263–274. <https://doi.org/10.1016/j.colsurfa.2014.05.057> (2014).
- Karimiyan, A., Najafzadeh, H., Ghorbanpour, M. & Hekmati-Moghaddam, S. H. Antifungal effect of magnesium oxide, zinc oxide, silicon oxide and copper oxide nanoparticles against *Candida albicans*. *Zahedan J. Res. Med. Sci.* **17**, e2179. <https://doi.org/10.17795/zjrms-2179> (2015).
- Vincent, M., Duval, R. E., Hartemann, P. & Engels-Deutsch, M. Contact killing and antimicrobial properties of copper. *J. Appl. Microbiol.* **124**, 1032–1046. <https://doi.org/10.1111/jam.13681> *Journal of Applied Microbiology* (2018).
- Martínez, A. *et al.* Dual antifungal activity against *Candida albicans* of copper metallic nanostructures and hierarchical copper oxide marigold-like nanostructures grown in situ in the culture medium. *J. Appl. Microbiol.* **130**, 1883–1892. <https://doi.org/10.1111/jam.14859> *Journal of Applied Microbiology* (2021).
- Powell, M. F. In *Annual Reports in Medicinal Chemistry* Vol. 28 (ed. Bristol, J. A.) 285–294 (Academic Press, 1993).
- Li, D. *et al.* N-terminal acetylation of antimicrobial peptide L163 improves its stability against protease degradation. *J. Pept. Sci.* **27**, e3337. <https://doi.org/10.1002/psc.3337> (2021).
- He, Z., Yuan, C., Zhang, L. & Yousef, A. E. N-terminal acetylation in paenibacillin, a novel lantibiotic. *FEBS Lett.* **582**, 2787–2792. <https://doi.org/10.1016/j.febslet.2008.07.008> (2008).
- Krishnakumari, V. & Nagaraj, R. N-terminal fatty acylation of peptides spanning the cationic C-terminal segment of bovine β -defensin-2 results in salt-resistant antibacterial activity. *Biophys. Chem.* **199**, 25–33. <https://doi.org/10.1016/j.bpc.2015.02.005> (2015).
- Pearson, R. G. Hard and soft acids and bases. *J. Am. Chem. Soc.* **85**, 3533–3539. <https://doi.org/10.1021/ja00905a001> (1963).
- Irving, H. & Williams, R. J. P. 637. The stability of transition-metal complexes. *J. Chem. Soc. (Resumed)* <https://doi.org/10.1039/JR9530003192> (1953).

40. Bellotti, D., Tocchio, C., Guerrini, R., Rowińska-Żyrek, M. & Remelli, M. Thermodynamic and spectroscopic study of Cu(II) and Zn(II) complexes with the (148–156) peptide fragment of C4YJH2, a putative metal transporter of *Candida albicans*. *Metallomics* **11**, 1988–1998. <https://doi.org/10.1039/c9mt00251k> (2019).
41. Gans, P., Sabatini, A. & Vacca, A. SUPERQUAD: An improved general program for computation of formation constants from potentiometric data. *Dalton Trans.* **6**, 1195–1200 (1985).
42. Gans, P. & O'Sullivan, B. GLEE, a new computer program for glass electrode calibration. *Talanta* **51**, 33–37. [https://doi.org/10.1016/s0039-9140\(99\)00245-3](https://doi.org/10.1016/s0039-9140(99)00245-3) (2000).
43. Gran, G. Determination of the equivalent point in potentiometric titrations. *Acta Chem. Scand.* **4**, 559–577. <https://doi.org/10.3891/acta.chem.scand.04-0559> (1950).
44. Gans, P., Sabatini, A. & Vacca, A. Investigation of equilibria in solution. Determination of equilibrium constants with the HYPERQUAD suite of programs. *Talanta* **43**, 1739–1753 (1996).
45. Brown, P. L. & Ekberg, C. *Hydrolysis of Metal Ions* 499–716 (Wiley, 2016).
46. Arena, G., Cali, R., Rizzarelli, E. & Sammartano, S. Thermodynamic study on the formation of the cupric ion hydrolytic species. *Therm. Acta* **16**, 315–321. [https://doi.org/10.1016/0040-6031\(76\)80024-X](https://doi.org/10.1016/0040-6031(76)80024-X) (1976).
47. Alderighi, L. *et al.* Hyperquad simulation and speciation (HySS): A utility program for the investigation of equilibria involving soluble and partially soluble species. *Coord. Chem. Rev.* **184**, 311–318 (1999).
48. Berto, S. *et al.* Oxovanadium(IV) coordination compounds with Kojic acid derivatives in aqueous solution. *Molecules* **24**, 3768. <https://doi.org/10.3390/molecules24203768> (2019).
49. Prenesti, E., Daniele, P. G., Prencipe, M. & Ostacoli, G. Spectrum-structure correlation for visible absorption spectra of copper(II) complexes in aqueous solution. *Polyhedron* **18**, 3233–3241. [https://doi.org/10.1016/S0277-5387\(99\)00279-X](https://doi.org/10.1016/S0277-5387(99)00279-X) (1999).
50. Billo, E. J. Copper(II) chromophores and the rule of average environment. *Inorg. Nuclear Chem. Lett.* **10**, 613–617. [https://doi.org/10.1016/0020-1650\(74\)80002-4](https://doi.org/10.1016/0020-1650(74)80002-4) (1974).
51. Benovitz, D. E. & Spatola, A. F. Enkephalin pseudopeptides: Resistance to in vitro proteolytic degradation afforded by amide bond replacements extends to remote sites. *Peptides* **6**, 257–261. [https://doi.org/10.1016/0196-9781\(85\)90049-X](https://doi.org/10.1016/0196-9781(85)90049-X) (1985).

Acknowledgements

This research was funded by the Polish National Science Centre (UMO-2020/37/N/ST4/03165-D.B.). Staff exchange was possible due to COST Action CA18202, NECTAR—Network for Equilibria and Chemical Thermodynamics Advanced Research, supported by COST (European Cooperation in Science and Technology). M.R. and E.C. are supported by University of Ferrara (FAR 2021, FIRD 2022).

Author contributions

D.B., M.D.A., M.R., E.C. and M.R.-Z. conceived and planned the experiments. D.B., M.D.A., E.D., C.L., S.L., V.A. and E.M. conducted the experiments. D.B., M.D.A., M.R., E.C., R.G. and M.R.-Z. analysed the results. D.B., M.D.A., M.R., E.C. and M.R.-Z. wrote the main manuscript. All authors reviewed the manuscript.

Competing interests

The authors declare no competing interests.


Additional information

Supplementary Information The online version contains supplementary material available at <https://doi.org/10.1038/s41598-023-45437-0>.

Correspondence and requests for materials should be addressed to D.B.

Reprints and permissions information is available at www.nature.com/reprints.

Publisher's note Springer Nature remains neutral with regard to jurisdictional claims in published maps and institutional affiliations.

 **Open Access** This article is licensed under a Creative Commons Attribution 4.0 International License, which permits use, sharing, adaptation, distribution and reproduction in any medium or format, as long as you give appropriate credit to the original author(s) and the source, provide a link to the Creative Commons licence, and indicate if changes were made. The images or other third party material in this article are included in the article's Creative Commons licence, unless indicated otherwise in a credit line to the material. If material is not included in the article's Creative Commons licence and your intended use is not permitted by statutory regulation or exceeds the permitted use, you will need to obtain permission directly from the copyright holder. To view a copy of this licence, visit <http://creativecommons.org/licenses/by/4.0/>.

© The Author(s) 2023